LEO MAPPING FOR PASSIVE DYNAMICAL DISPOSAL

E. M. Alessi[(1)], G. Schettino[(1)], A. Rossi[(1)], and G. B. Valsecchi[(2)]

[(1)]*Istituto di Fisica Applicata "Nello Carrara" – Consiglio Nazionale delle Ricerche, via Madonna del Piano 10, 50019 Sesto Fiorentino (FI), Italy, Email: em.alessi@ifac.cnr.it, g.schettino@ifac.cnr.it, a.rossi@ifac.cnr.it*
[(2)]*IAPS-INAF, via Fosso dei Cavalieri 100, 00133 Rome (Italy), Email: giovanni@iaps.inaf.it*

ABSTRACT

The growth of the number of space objects in the Low Earth Orbit (LEO) region requires both the implementation of prevention strategies and the outline of advanced re-entry solutions. By means of a dedicated orbit propagator, we studied the dynamics of sample objects over 120 years, in a dense grid of orbital elements covering the whole LEO phase space, considering two initial epochs. Beyond the standard area-to-mass ratio of typical payloads in LEO, we also assumed the use of area augmentation devices. The final goal of this analysis is to take advantage of the dynamical instabilities induced by orbital perturbations to reduce the residual lifetime of disposed spacecraft. The output of the simulations highlighted that the orbital perturbations due to geopotential, lunisolar perturbations and solar radiation pressure can significantly change the eccentricity of the orbit at selected inclinations bands. A Fourier transform analysis confirmed the role of given resonances in the eccentricity evolution as a function of the initial orbital elements. An impulsive strategy to move the spacecraft at end-of-life towards the unstable zones is also sketched.

Key words: LEO; resonances; SRP; passive disposal; end-of-life strategy.

1. INTRODUCTION

The increasing instability of the Low Earth Orbit (LEO) region requires the planning of end-of-life measures since the very early phases of the mission design. To avoid the accumulation of spent, uncontrolled spacecraft in a restricted region of space, which would lead inevitably to a significant number of collisions, it is mandatory to look for solutions which aim at reentering to the Earth rather than exploiting graveyard orbits. The first step towards this direction is to understand if the dynamical perturbations in the region can drive the spacecraft towards natural reentry highways. Passive solutions of this kind will be preferred if they result to be energetically more convenient than a maneuver towards a graveyard orbit, and achievable in a reasonable time frame (in principle, according to the well-known 25-year rule). This, in turn, means a solution which results affordable for the space operators and not risky for the space environment.

Having this objective in mind, in the framework of the ReDSHIFT H2020 project, we performed an extensive numerical simulation in order to detect the maximum variations in each orbital element over a time interval of 120 years. The fine grid of initial conditions covers the whole LEO region up to graveyard orbits altitudes, for prograde and retrograde orbits, and from very circular up to very eccentric orbits. Beyond the altitudes where the atmospheric drag is effective as much as to lead eventually to a reentry, the main mechanism which might help to reduce the lifetime of a satellite is the eccentricity growth, caused by either the solar radiation pressure (SRP) or the lunisolar perturbations. The analysis of the numerical results, but also a dedicated frequency analysis, confirmed the existence of dynamical resonances associated with these effects. According to the initial value of semi-major axis and inclination, and to the area-to-mass value of the object, these resonances might be exploited to leverage the instability of the orbit, and move the spacecraft towards the region where the drag is effective to achieve reentry.

2. DYNAMICAL MAPPING

The dynamical mapping of the LEO region was obtained by propagation of the initial conditions in semi-major axis a, eccentricity e and inclination i, displayed in Table 1 for a maximum time span of 120 years. The longitude of the ascending node Ω and the argument of pericenter ω were sampled at a step of 90° starting from 0°. The initial epochs considered are December 22, 2018 at 17:50:21, and June 21, 2020 at 06:43:12, and the area-to-mass ratio $A/m = 0.012$ m^2/kg, which represents the average value of the orbiting intact bodies. The same simulation was repeated for the epoch 2020 assuming $A/m = 1$ m^2/kg, which represents an achievable value for a drag- or SRP-enhancing device with the present technology.

The numerical method adopted is the Fast Orbit Propagator (FOP) [1, 7], which is an accurate, long-term orbit predictor, based on the Long-term Orbit Predictor (LOP)

a (km)	Δa (km)	e	Δe	i (deg)	Δi (deg)
$[500-700]$ + R_E	50	$[0:0.28]$	0.01	$[0:120]$	2
$[700-1000]$ + R_E	20	$[0:0.28]$	0.01	$[0:120]$	2
$[1000-1300]$ + R_E	50	$[0:0.28]$	0.01	$[0:120]$	2
$[1300-1600]$ + R_E	20	$[0:0.28]$	0.01	$[0:120]$	2
$[2000-3000]$ + R_E	100	$[0:0.28]$	0.01	$[0:120]$	2

Table 1. Grid in semi-major axis a, eccentricity e and inclination i assumed as initial conditions for the exploration performed. R_E is the radius of the Earth.

[6]. FOP integrates singly-averaged equations of motion for a set of orbital elements, which are non-singular for circular orbits and singular only for equatorial orbits. The numerical integrator is a multi-step, variable step-size and order one. The dynamical model includes the gravitational contributions due to Earth (5×5 geopotential), Moon and Sun (as third-body perturbations), as long as solar radiation pressure and atmospheric drag. The SRP effect is defined by the cannonball model, accounting also for shadowing intervals. The atmospheric drag is applied for altitudes below 1500 km, adapting the Jacchia-Roberts density model assuming an exospheric temperature of 1000 K and a variable solar flux at 2800 MHz (obtained by means of a Fourier analysis of data corresponding to the interval 1961-1992). The reflectivity coefficient was set as $C_R = 1$ or $C_R = 2$ depending on the simulation, while the drag coefficient as $C_D = 2.1$.

During the numerical propagation, the maximum and minimum values computed in semi-major axis, eccentricity and inclination were recorded, along with the corresponding epoch. A reentry was assumed to occur whenever the altitude got below 300 km.

To deepen our analysis, we performed a further characterization of the considered orbits in terms of their periodic components. Within the grid defined in Table 1, we decomposed the quasi-periodic time series of each orbital element, obtained by propagation with FOP, in their spectral components. This decomposition was derived by means of a numerical computation of the Fourier transform, accounting for the finite duration of the signals. As a starting point, we removed from the dynamical model the lunisolar perturbations and we focused on the SRP effects. The aim of this spectral analysis is to link clearly each frequency signature to the dynamical effect which generates it. Together with the analysis of the temporal evolution of the orbits, the frequency mapping will assist in achieving a complete and detailed characterization of the LEO region.

3. DYNAMICAL CORRIDORS

The results obtained from the exploration just described were analyzed, first of all, by means of color maps, which represent either the maximum eccentricity or the lifetime computed as a function of the initial inclination and eccentricity (or pericenter altitude) for all the values of initial semi-major, longitude of ascending node, argument of pericenter, epoch and area-to-mass ratio. An example for both area-to-mass ratios is shown in Figures 1 and 2.

This approach allowed to detect resonant corridors, where the eccentricity may be induced to grow, depending on the initial orbital configuration. In particular, solar radiation pressure and lunisolar perturbations cause long-term periodic variations in eccentricity, which become quasi-secular when a resonance involving the rate of Ω and ω occurs. In LEO, for the two values of area-to-mass ratio adopted, we can assume that ω and Ω vary only because of the oblateness of the Earth, and thus the corresponding rates depend only on (a, e, i). This fact explains the stripes that can be distinguished in Figures 1 and 2 in correspondence of well-defined values of inclination, given the initial value of the other parameters.

For low values of A/m, if n_S is the mean apparent motion of the Sun, our analysis revealed that the main resonances in LEO are:

- $\alpha\dot{\Omega} + 2\dot{\omega} + \beta n_S \approx 0$, with $\alpha = 0, 1, 2$ and $\beta = 0, \pm 1, -2$, due to lunisolar perturbations (e.g., [5]);
- $\dot{\omega} \approx 0$, due to zonal terms of degree 3 and 5 (e.g., [8]) in the geopotential, but also with lunisolar perturbations (e.g., [5]);
- $\alpha\dot{\Omega} \pm \dot{\omega} \pm n_S \approx 0$, with $\alpha = 0, 1$ due to SRP [3, 4],

where

$$\dot{\Omega} = -\frac{3}{2}\frac{J_2 R_E^2 n}{a^2(1-e^2)^2}\cos i,$$
$$\dot{\omega} = \frac{3}{4}\frac{J_2 R_E n}{a^2(1-e^2)^2}\left(5\cos^2 i - 1\right),$$

being J_2 the second zonal term and n the mean motion of the satellite (see, e.g., [2]). For the high value of A/m considered in this work, only the third type of resonances plays a significant role in the eccentricity evolution.

The maps highlight some symmetries in the argument of the given resonance. Let us look to Figure 3 and Figure 4, which describe the behavior of the maximum eccentricity

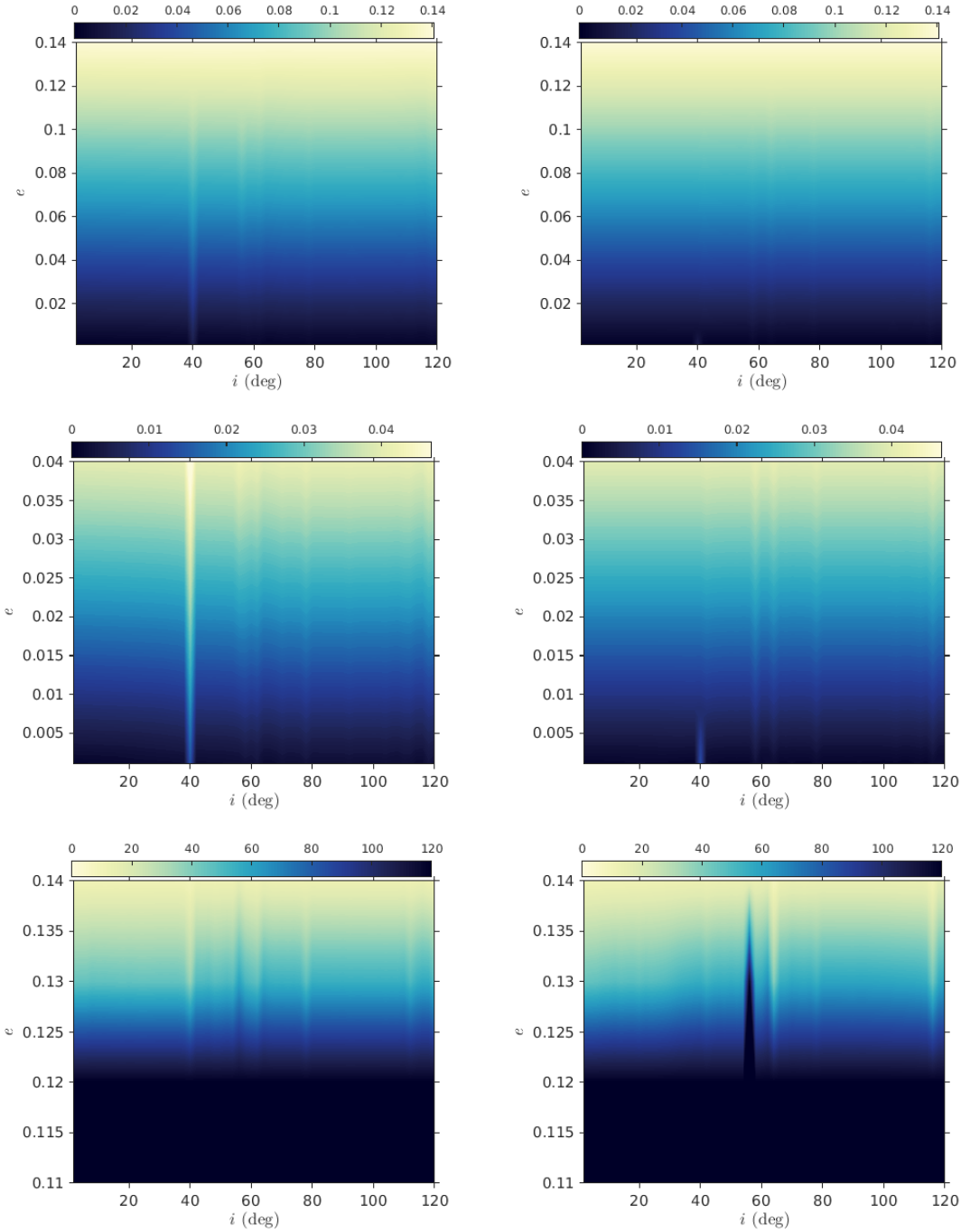

Figure 1. The color bar shows the maximum eccentricity (top and middle plots) and the lifetime (bottom plots) computed over 120 years as a function on initial inclination and eccentricity, considering an initial semi-major axis $a = R_E + 1400$ km, the initial 2020 epoch and $C_R A/m = 0.024$ m^2/kg. Left: $\Omega = 0°$, $\omega = 90°$. Right: $\Omega = 90°$, $\omega = 180°$. The middle plots represent a close-up for circular orbits.

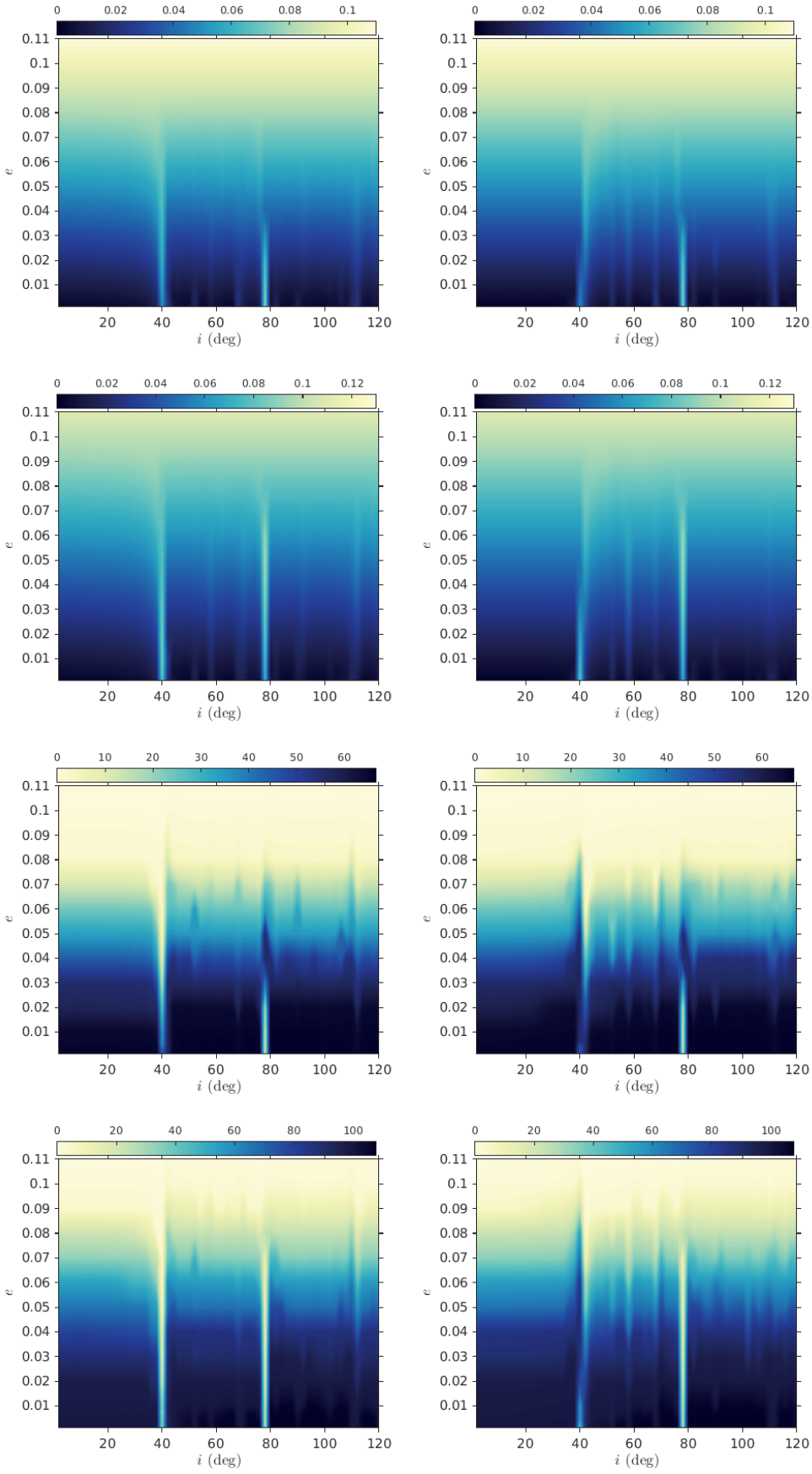

Figure 2. The color bar shows the maximum eccentricity (rows 1 and 2) and the lifetime (rows 3 and 4) computed over 120 years as a function on initial inclination and eccentricity, considering the initial 2020 epoch and $C_R A/m = 1\ m^2/kg$.

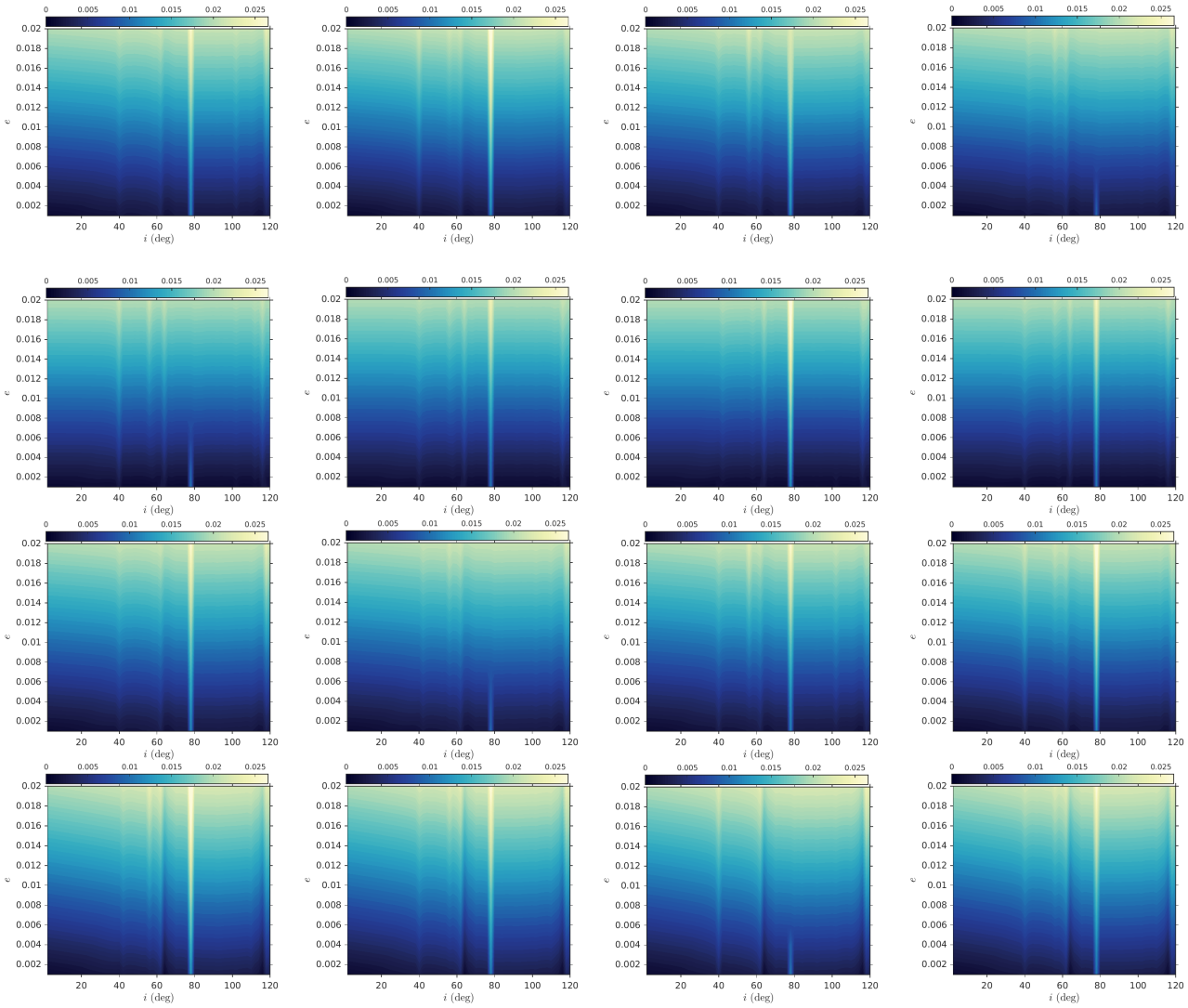

Figure 3. Maximum eccentricity over 120 years as a function on initial inclination and eccentricity, considering an initial semi-major axis $a = R_E + 1250$ *km, the initial 2020 epoch and* $C_R A/m = 0.024$ m^2/kg*. From top to bottom:* $\Omega = 0°, 90°, 180°, 270°$*; from left to right:* $\omega = 0°, 90°, 180°, 270°$.

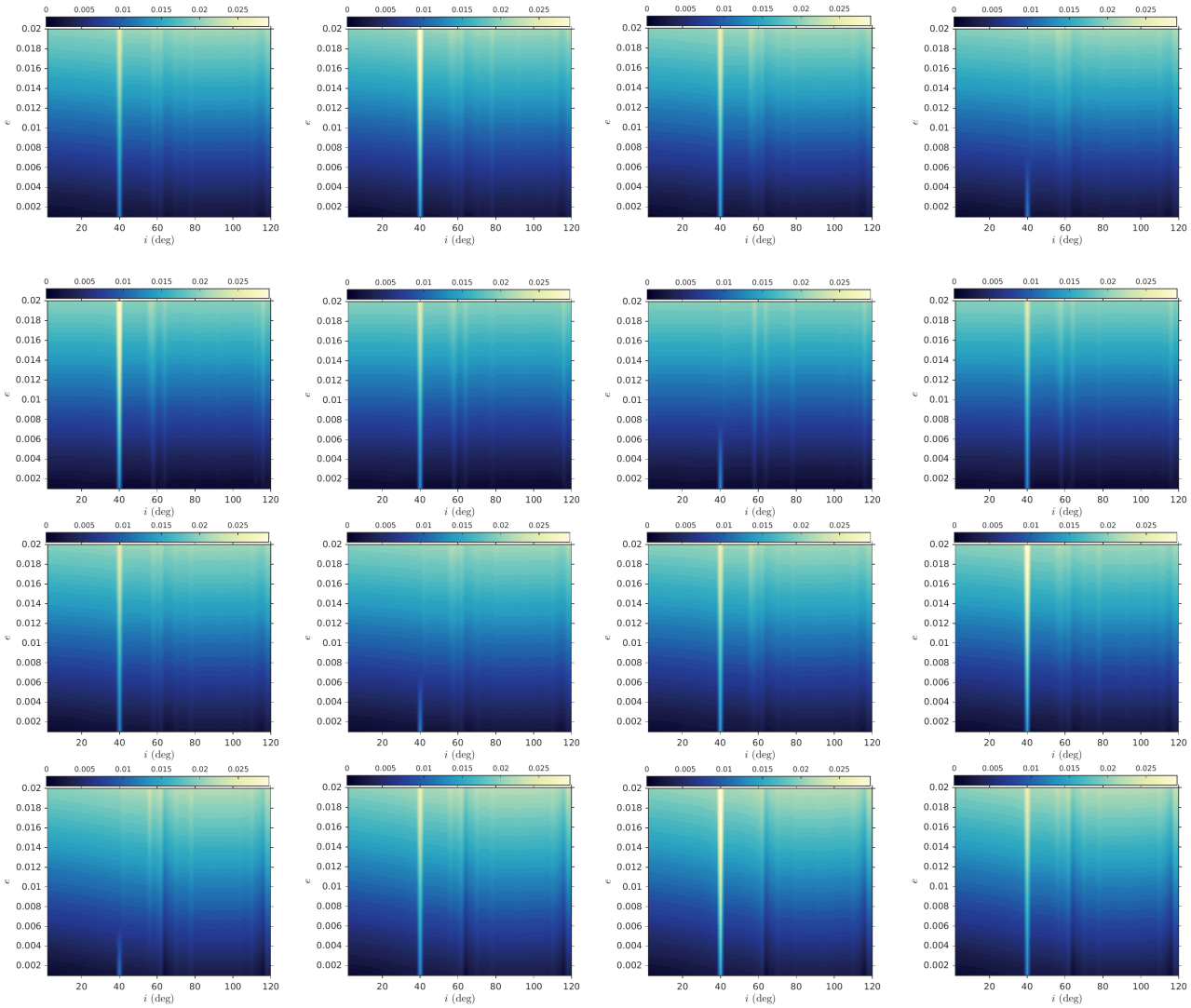

Figure 4. Maximum eccentricity over 120 years as a function on initial inclination and eccentricity, considering an initial semi-major axis $a = R_E + 1400$ km, the initial 2020 epoch and $C_R A/m = 0.024$ m^2/kg. From top to bottom: $\Omega = 0°, 90°, 180°, 270°$; from left to right: $\omega = 0°, 90°, 180°, 270°$.

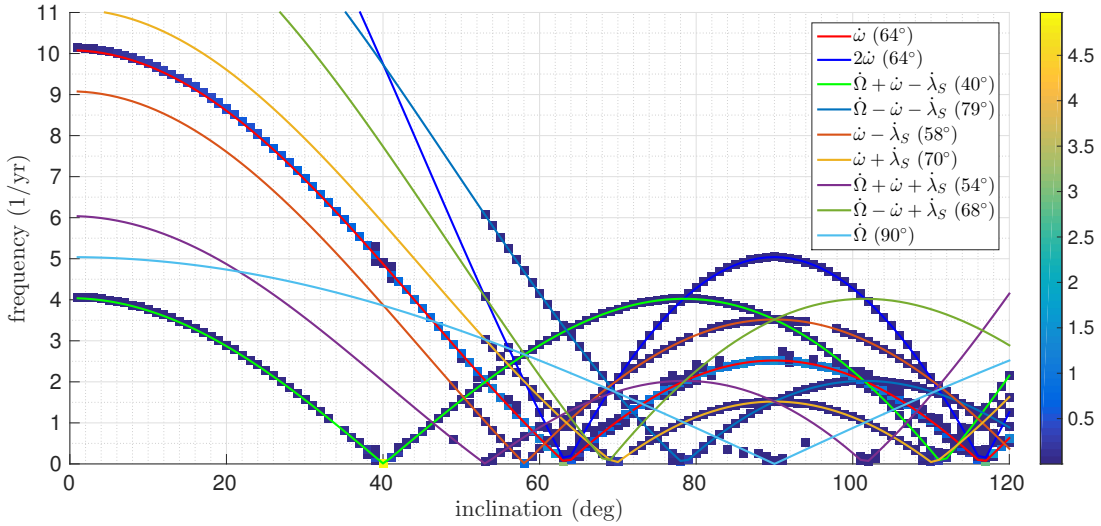

Figure 5. Plot of the frequencies detected in the spectrum of the eccentricity series for the case $e = 0.02$, $a = R_E + 1400$ km, $\Omega = 0°$, $\omega = 90°$, $C_R A/m = 0.024\,m^2/kg$ and epoch 2020. The color bar scans the amplitude of the spectral signatures. The curves shown correspond to the resonances of second and third type (see text). Comparing the relative amplitude of the spectral signatures, we can see that the most important term is due to the $\dot{\Omega} + \dot{\omega} - n_S \approx 0$ due to SRP at about $i \approx 40°$ (yellow marker), followed by the $\dot{\omega} \approx 0$ resonance due to geopotential around $i \approx 64°$ and $i \approx 116°$ (green marker) and the $\dot{\omega} - n_S \approx 0$ due to SRP at $i \approx 58°$ (light blue marker).

for quasi-circular orbits as a function of initial (i, e) for $a = R_E + 1250$ km and $a = R_E + 1400$ km, respectively, for each of the 16 (Ω, ω) combinations, assuming $A/m = 0.012$ m^{2}kg and the initial epoch 2020. These are illustrative cases, where we can observe that the variation detected depends on the initial value of Ω, ω (and the longitude of the Sun measured on the ecliptic plane, say λ_S). We first notice that, in the range of eccentricity considered, for $a = R_E + 1250$ km, the dominant resonance occurs at $i \approx 79°$: this is $\dot{\Omega} - \dot{\omega} - n_S \approx 0$ and it is due to the SRP. At $a = R_E + 1400$ km, instead, the main resonance is $\dot{\Omega} + \dot{\omega} - n_s \approx 0$, at $i \approx 40°$, also due to SRP. Looking to the figures, it is clear that we do not have 16 different color maps, i.e., the inclination corridors corresponding to a given resonance manifest the same behavior for different (Ω, ω) combinations. In particular, the same eccentricity variation is ascribable to three cases:

1. $\Omega \pm \omega - n_S = 0°$;
2. $\Omega \pm \omega - n_S = \pm 90°$;
3. $\Omega \pm \omega - n_S = 180°$,

where the sign in the argument depends on the resonance. Notice that we cannot state that a given case leads to a growth, while another to a decrease. This depends also on the initial eccentricity. For example, looking to the panels in Figure 3, when $\Omega - \omega - \lambda_S = 0°$ (e.g., first panel on the second row, where $\Omega = 90°$ and $\omega = 0°$, or second panel on the third row, where $\Omega = 180°$ and $\omega = 90°$) the eccentricity grows only up to $e = 0.008$.

Focusing on the eccentricity evolution under the SRP perturbation, we performed an analysis of the frequency components which characterize the eccentricity time series, as a function of the inclination, fixing (a, Ω, ω), the area-to-mass ratio and the initial epoch. We are interested in the spectral signatures at the inclinations corresponding to SRP resonances. Theory provides for them characteristic periods of the order of year or tens of years, depending on the specific resonance and on (a, e). Thus, in order to obtain an accurate numerical Fourier transform, we need to propagate the orbits over a suitable time window, longer than 120 years. Moreover, we sampled the inclination at a step of $0.5°$ in the $[2 : 120]°$ range in order to have a finer grid especially around the resonances. An example of this kind of analysis for $e = 0.02$, $a = R_E + 1400$ km, $\Omega = 0°$, $\omega = 90°$ for the case $C_R A/m = 0.024\,m^2/kg$ and epoch 2020 is shown in Figure 5. Each marker represents a frequency component detected in the eccentricity time series at a specific value of inclination by means of the numerical Fourier transform; the color bar scans the amplitude of the spectral signatures. The lines corresponding to the resonance of the second type, due to geopotential (together with its second harmonic), and to the main resonances of the third type, due to SRP, are shown in the plot: as it can be seen, the detected frequencies are laid well along the theoretical curves. Most of the resonances exhibits two singularities in the $[2 : 120]°$ selected range of inclinations. Note also that the markers around $i = 90°$ do not fit with any of the mentioned resonances, but they correspond to the curve associated with the higher order resonance $\dot{\Omega} \approx 0$

due to SRP.

The amplitude of each frequency signature allows to identify which resonances are dominant, at the selected (a, Ω, ω). In the case of Figure 5, comparing the amplitudes of the spectral signatures corresponding to the resonances, the main term belongs to the $\dot{\Omega} + \dot{\omega} - n_S \approx 0$ resonance due to SRP around $i \approx 40°$ (yellow marker), followed by the $\dot{\omega} \approx 0$ resonance due to geopotential around $i \approx 64°$ and $i \approx 116°$ (green marker) and the $\dot{\omega} - n_S \approx 0$ resonance due to SRP at $i \approx 58°$ (light blue marker). We expect that this analysis reproduces the behavior identified in the maximum eccentricity maps. Comparing with Figure 1-left, which represents the maximum eccentricity evolution at the same initial conditions $a = R_E + 1400$ km, $\Omega = 0°$, $\omega = 90°$, the signature around $i \approx 40°$ appears to be the brightest one and the other signatures found in the spectral analysis appear as fainter stripes.

In general, for low area-to-mass values, the effect of the resonances is not able on its own to drive the satellite to achieve reentry. In particular, considering values of semi-major axis for which the lifetime of a circular orbit is generally higher than 100 years ($\approx$ 800 km of altitude), a resonance could be used to decrease the pericenter altitude as much as to be able then to exploit the shrinking effect caused by the atmospheric drag. The effect detected for $A/m = 1$ m^2/kg is different, in the sense that there exist initial quasi-circular orbits at an altitude up to about 1950 km (see Figure 6) which can reenter thanks only to the resonances associated with SRP, which also means along well-defined inclination highways.

Note that among the findings of this work, there is also a new insight on the boundary between the atmospheric drag and the SRP effects for high values of area-to-mass ratio. From Figure 2, we can deduce, in particular, that for circular orbits at 1300 km of altitude the drag does not play any role, while at 1200 km it still does.

4. CONCLUSIONS AND FUTURE DIRECTIONS

We presented the results of an extended and systematic analysis on the dynamics characterizing the LEO region, analysis not existing so far. The outcome represents an accurate description of the long-time behavior in semi-major axis, eccentricity and inclination, which can be used, in particular, for the design of passive disposal solutions. The numerical and theoretical analysis revealed that the LEO region is pervaded by gravitational and non-gravitational resonances, which can exploited to reduce in a natural way the lifetime of the objects.

If a given initial condition does not allow to reenter in an operational time interval, i.e., the semi-major axis is not low enough, or the eccentricity is too low, or the inclination does not correspond to a resonant corridor, it might be still possible to take advantage of the results obtained by adopting an impulsive strategy at a suitable epoch.

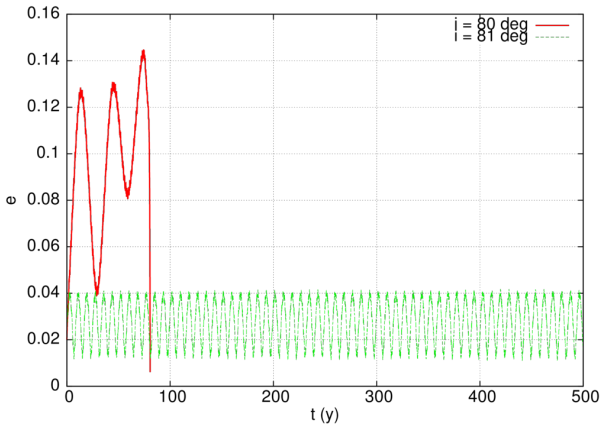

Figure 6. Eccentricity evolution considering $C_R A/m = 1\ m^2/kg$ and starting from $a = R_E + 1950$ km, $e = 0.02$, $\Omega = 270°$, $\omega = 270°$, epoch 2020 and two neighboring values of inclination: $i = 80°$ (red curve) which corresponds to a SRP resonance, and $i = 81°$ (green curve) which does not.

Given an initial condition, Gaussian equations (see, e.g., [2]) can be applied to target points in the maps which turn out to be advantageous compared to their neighbors and to a simple deorbiting maneuver. The maximum and minimum values stored can be used to optimize the approach, making precise assumptions on the role of the initial epoch in the evolution of the orbit. The Fourier analysis and the data obtained for the epoch 2018 will help in this choice.

ACKNOWLEDGMENTS

This work is funded through the European Commission Horizon 2020, Framework Programme for Research and Innovation (2014-2020), under the ReDSHIFT project (grant agreement n° 687500).

REFERENCES

1. Anselmo, L., Cordelli, A., Farinella, P., Pardini C., & Rossi, A. , (1996). Study on long term evolution of Earth orbiting debris, ESA/ESOC contract No. 10034/92/D/IM(SC).

2. Battin, R. H., (1999). *An Introduction to the Mathematics and Methods of Astrodynamics*, Revised Edition, AIAA Education Series, American Institute of Aeronautics and Astronautics, Inc., Reston.

3. Cook, G. E., (1962). Luni-solar Perturbations of the Orbit of an Earth Satellite, *The Geophysical Journal of the Royal Astronomical Society*, **6**, 271–291.

4. Hughes, S., (1977). Satellite orbits perturbed by direct solar radiation pressure: general expansion of the

disturbing function, *Planetary and Space Science*, **25**, 809–815.

5. Hughes, S., (1980). Earth Satellite Orbits with Resonant Lunisolar Perturbations. I. Resonances Dependent Only on Inclination. *Proceedings of the Royal Society of London. Series A, Mathematical and Physical Sciences*, **372**, 243–264.

6. Kwok, J. H., (1986). The long-term orbit prediction (LOP), JPL Technical Report EM 312/86-151.

7. Rossi, A., Anselmo, L., Pardini, C., Jehn, R., & Valsecchi, G. B., (2009). The new space debris mitigation (SDM 4.0) long term evolution code, Proceedings of the Fifth European Conference on Space Debris, Darmstadt, Germany, Paper ESA SP-672.

8. Roy, A. E., (2005). *Orbital Motion*, Institute of Physics Publishing, Bristol.